4

Specific Applications of Vibrational Spectroscopy in Biomedical Engineering

Sylwia Olsztyńska-Janus[1],
Marlena Gąsior-Głogowska[1,4], Katarzyna Szymborska-Małek[2],
Bogusława Czarnik-Matusewicz[3] and Małgorzata Komorowska[1,4]
[1]*Institute of Biomedical Engineering and Instrumentation, Wrocław University of Technology,*
[2]*Institute of Physical and Theoretical Chemistry, Wrocław University of Technology,*
[3]*Faculty of Chemistry, University of Wrocław,*
[4]*Regional Specialist Hospital in Wrocław, Research and Development Centre, Wrocław, Poland*

1. Introduction

Nucleic acids such as proteins, amino acids, lipids and carbohydrates are located, as the basic components of animal cells, plant cells and microorganisms, in many cellular organelles. In eukaryotic organisms, deoxyribonucleic acid (DNA) is found in the cell nucleus, mitochondria and chloroplasts, while ribonucleic acid (RNA) occurs mainly in the cytoplasm of the cell. In prokaryotes such as bacteria and archaea, DNA is also found in the cytoplasm of the cell. Nucleic acids play an important role in storage, transfer and incorporation of genetic information into the cell. DNA contains the genetic codes to make RNA, while RNA contains the codes for the primary sequence of amino acids for protein synthesis, which plays a fundamental role for living creatures (Campbell & Farrell, 2009).
Fundamental vital processes occur at the molecular level, therefore research methods allowing for investigation of molecular processes are crucial in their understanding. Vibrational (Infrared and Raman) Spectroscopy is used to obtain both structural and conformational information of biological systems, including amino acids, proteins and lipids (Barth, 2007; Byler & Susi, 1986; Cieślik-Boczula et al., 2007; Murawska et al., 2010; Murayama et al., 2001; Szwed et al., 2010; Szyc et al., 2008; Wolpert & Heellwig, 2006; Wu et al., 2002). Raman spectroscopy seems also to be a very powerful tool for the study of stress-induced molecular changes in both natural and synthetic polymers (Amer, 2009; Koening, 2001). This technique has been applied for such tissues as tendon, blood vessel walls and skin. Simple correlation between the Raman spectroscopic data and mechanical relations can be established (Hanuza et al., 2009; Winchester et al., 2008).
Temperature, pH, presence of salts, electromagnetic radiation exposure and organic solvents modify biological compounds, inducing specific conformational changes which are relevant for the understanding of their functions (Parker, 1983). Vibrational spectroscopy has been applied to study cells or molecules in tissues changed by various factors. It is therefore frequently used as a diagnostic tool in pharmacy (Wartewig & Neubert, 2005), in cancer

research (Amharref et al., 2007; Li et al., 2005), in neurological disorders and diseases of the cardiovascular system (Pysz et al., 2010) and in bone diseases (Fuchs et al., 2008), as well as in Alzheimer's disease (Griebe et al., 2007). It allows the progress of these diseases and the effectiveness of therapy to be monitored. It is necessary to use measuring techniques which make it possible to reach the micro- and even nanoareas of tissue or enable the structure and properties of single molecules to be examined.

One of the most important infrared spectroscopy methods used in studies of biological systems is Attenuated Total Reflection (ATR) Fourier Transform Infrared (FTIR). The ATR accessory operates by measuring the absorption when a totally internally reflected infrared beam comes into contact with a sample. This technique provides a powerful and sensitive approach able to reveal changes in the biochemical properties of biomedical samples studied at the molecular level (Olsztynska et al., 2006a; Olsztynska et al., 2001). It enables study of the relative concentrations of individual components of tissue and inter- or intramolecular interactions between them. Many substances in the solid and liquid state can be characterized, identified and also quantified by FTIR-ATR spectroscopy (Heise et al., 2002). Studies of tissue can be carried out on thin sections with a thickness of several micrometers. In the case of liquid samples a few micro litres of fluid are sufficient for measurements. Typically, tissue samples are collected during a biopsy, endoscopy or puncture, or from intraoperative material used for this purpose. One of the key advantages of FTIR-ATR is that studies can be conducted on a small amount of biomedical material. Another is not needing to use additional reagents or biological markers, which significantly reduces sample preparation time and reduces the cost of analysis. Research material downloaded without fixation, dyeing and additional chemical treatment can be almost immediately analysed. FTIR with an ATR accessory has shown to be a very valuable tool in pharmaceutical (McAuley et al., 2009) and polymer (Licoccia et al., 2005) applications. Tissue or tissue components having been characterized by FTIR-ATR spectroscopy are human hair (Chan et al., 2005), biological fluids including blood (Damm et al., 2007; Heise et al., 1989), and cancer tissue (Sun et al., 2003).

2. Vibrational spectroscopy of macromolecules; amino acids, proteins and DNA

2.1 Amino acids

Amino acids (AAs) are the basic building blocks of peptides and proteins. As they belong to the simplest class of biomolecules, detailed investigation of their properties and interactions is essential for understanding the behaviour of macromolecules in different circumstances. Despite the fact that physiological processes occur in the aqueous phase, measurements of AAs are often performed in the solid state (Medien, 1998), which does not provide information about effects occurring in aqueous solutions. Even a newly developed dissolution-spray-deposition infrared technique (Cao & Fischer, 1999) is no help in understanding biological processes at the molecular level. AAs are not easily studied by vibrational spectroscopy, in that the vibrational bands of AAs in aqueous solution are usually broad, overlapped or even incomplete as a result of strong solvent absorption, particularly that arising from water, and solute-solvent interactions. It is well known that AAs may exist in various protonation states, which are clearly reflected in the vibrational spectra. Wolpert and Hellwig (Wolpert & Hellwig, 2006) have presented spectra of AA head groups in different protonation states and made detailed assignments for the 20 alpha AAs

in aqueous solution in the range 1800-500 cm^{-1}. The IR spectra of glycine in aqueous solutions obtained in the pH range 0.2-14 allow charge distribution on the molecule to be determined (Max et al., 1998).

For example, presented in Figure 1 are the FTIR-ATR spectra of different AAs, i.e. L-glycine (Gly), L-alanine (Ala) and L-phenylalanine (Phe), in aqueous solution obtained in the region 1800–800 cm^{-1}. Tentative assignments of the main infrared bands of these three AAs are summarized in Table 1.

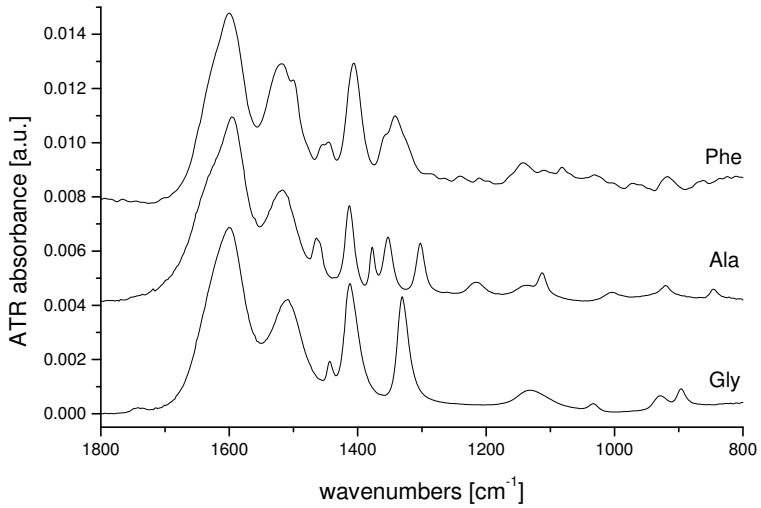

Fig. 1. FTIR-ATR spectra of L-glycine (Gly), L-alanine (Ala) and L-phenylalanine (Phe) in aqueous solution obtained in the region 1800–800 cm^{-1}. The spectra are shifted in absorbance for clarity.

Gly	**Ala**	**Phe**	**Assignments***
1614 sh	1620 sh	1628 sh	$\beta_{as}(NH_3^+)$
1601	1597	1583	$\nu_{as}(CO_2^-)$
1509	1516	1528	$\beta_s(NH_3^+)$
		1448	$\beta_s(CH_2)$
1412	1412	1408	$\nu_s(CO_2^-$
	1373	1364	$\beta_s(CH_2)$
	1353		$\beta_s(CH_2)$
1331		1340	$\beta_s(CH_2)$
1131	1138	1131 sh	$\rho(NH_3^+)$
929	919	913	$\gamma(CH_2)$

*Abbreviations: ν, stretching; β, in-plane bending; γ, out-of-plane bending; ρ, rocking; s, symmetrical; as, asymmetrical; sh, shoulder.

Table 1. Major positions (in cm^{-1}) and tentative assignment of IR bands of aqueous Gly, Ala and Phe.

2.2 Proteins

There are several experimental methods available for determination of protein secondary structure, such as circular dichroism (CD) (Shanmugam & Polavarapu, 2006), nuclear magnetic resonance (NMR) (Sun et al., 2005), X-ray scattering and diffraction (Sun et al., 2005), calorimetry and fluorescence (Gelamo et al., 2002), diffuse reflectance (DR) (Ishida & Griffiths, 1993), electron paramagnetic resonance ESR (Gelamo et al., 2004), Raman (Bolton & Scherer, 1989), near infrared (NIR) (Wu et al., 2000) and IR spectroscopy (Cai & Singh, 1999; Grdadolnik & Maréchal, 2001a & 2001b; Jackson et al., 1989; Maréchal, 2004 & 2003; van de Weert et al., 2001; Zhang & Yan, 2005). The last has for many years been a promising technique for the determination of the secondary structure of proteins in that some peptide vibrations are sensitive to conformation (Harris & Chapman, 1992; Jackson & Mantsch, 1995). In particular, FTIR-ATR has recently been applied for rapid analysis (Jeyachandran et al., 2009; Pevsner & Diem, 2001; Smith et al., 2002; Wang et al, 2003).

Of particular interest in interpreting infrared spectra of proteins are the amide I, II and III bands. These can be described as a function of backbone coordinates, as shown in Table 2. The three amide bands are usually a superposition of several individual components of the different secondary structure elements. It is possible to identify them only with the mathematical procedures for band resolution, i.e. derivative spectroscopy (Zhang & Yan, 2005) and Fourier self-deconvolution (Byler & Susi, 1986). The component bands can be assigned to specific secondary structures, such as α helix, β sheet, β turns or random coil (Byler & Susi, 1986). Frequencies of amide I vibrations for the most popular secondary structures are collected in Table 3.

	Designation	Approximate frequency (cm^{-1})	Assignment and PED*
Amide	A	3300-3230	ν(NH) 100%
	B	~ 3100	ν(NH) 100%
	I	1700-1600	ν(CO) 70-85% ν(CN) 10-20%
	II	1580-1510	δ(NH) 40-60% ν(CN) 18-40%; ν($C^{\alpha}C^{sch}$) ~10%
	III	1400-1200	δ(NH) 10-40% ν(CN) 0-40%; ν($C^{\alpha}C^{sch}$) 0-20%

*Abbreviations: PED, potential energy distribution; ν, stretching; δ, in-plane bending; sch, side chain.

Table 2. Summary of the characteristic bands associated with the peptide group.

Most methods used to determine the secondary structure of peptides and proteins concentrate on an analysis of the amide I (Dong et al., 1990), amide I and II (Dousseau & Pézolet, 1990), or amide III bands (Cai & Singh, 2004; Fabian & Mäntele, 2002; Fu et al., 1994).

Selected as a model protein was bovine serum albumin (BSA), which belongs to a major class of animal proteins. BSA is free of prosthetic groups and other complicating factors, and its primary, secondary and tertiary structure has been well-characterized. When FTIR-ATR spectroscopy is combined with derivative and difference spectroscopy procedures, it is possible to monitor even small changes in the conformation of a BSA protein in aqueous

solution affected by any factor. The FTIR-ATR spectra of BSA in an aqueous solution with concentrations of 10 wt % are presented in Figure 2 in the range of the three amide bands.

Secondary structure	Position of Amide I band (cm^{-1}) v(C=O)
α helix	1660-1648
β sheet	1640-1625 (strong absorption) 1690 (weak absorption)
β turns	1685-1660
random coil	1660-1652
β turns (3_{10}-helix)	1670-1660
aggregated	1628-1610

Table 3. Frequencies of amide I vibrations for different secondary structures.

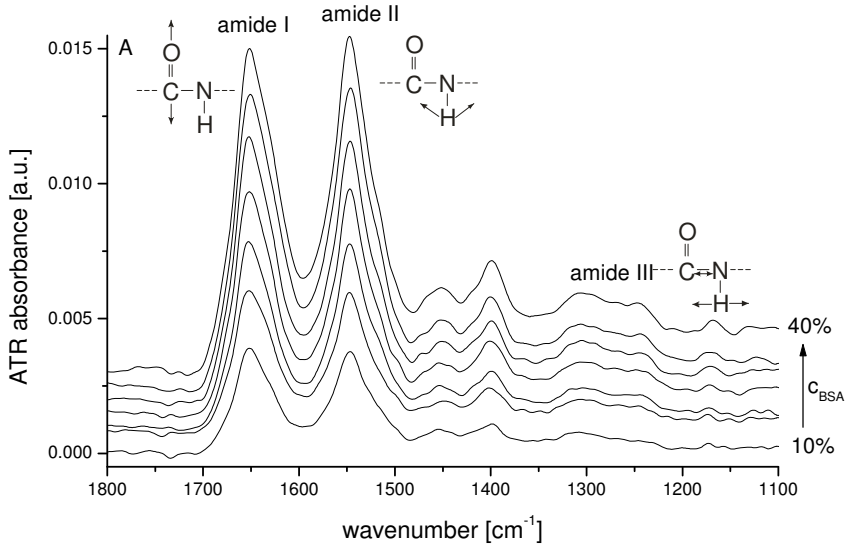

Fig. 2. FTIR-ATR spectra in the region 1800–1100 cm^{-1} of BSA in aqueous solutions at different concentrations (10, 15, 20, 25, 30, 35 and 40 wt %). The spectra were constructed using the water spectrum as the background. The spectra are shifted in absorbance for clarity.

FTIR-ATR spectroscopy was applied to study the effect of pH and metal ions on the conformation of BSA in aqueous solution (Qing et al., 1996). Small effects of binding with metal ions can also be detected by the splitting of the conformation-sensitive amide I band (Ahmed & Tajmir-Riahi 1993; Prestrelski et al., 1991). Ozaki's group investigated pH and heat-induced changes in the secondary structures of human serum albumin (HSA) and in the hydrogen bondings of side chains by two-dimensional/ATR correlation spectroscopy (Wu et al., 2002; Murayama et al., 2001). The ATR technique has been also used for

investigation of protein films, including thin hydrated films of soluble and membrane protein in a phospholipid bilayer (Goormaghtigh et al., 1990).

2.3 DNA

Raman and IR spectroscopies can be used to examine both short oligonucleotides and large structures of DNA. It is possible to study DNA samples in a solution, dehydrated fibre, film or crystalline form (Prescott et al., 1984; Taillandier et al., 1989; Taillandier & Liquier, 1992). Different factors, such as temperature, pH (Tajmir-Riahi et al., 1995), varying hydration (Falk et al., 1963; Lee et al., 2004; Pevsner & Diem, 2003; Tao et al., 1989) and ionic strength (Keller & Hartman, 1986; Taillandier et al., 1989, Taillandier & Liquier, 1992), affect the physical state of DNA samples.

2.3.1 IR spectroscopy

Vibrational spectroscopy is one of the main methods used to determine the secondary structures of A, B, C, D and Z-DNA forms (Banyay et al., 2003; Pohle & Fritzsche, 1980; Rauch et al., 2005; Taboury et al., 1985; Taillandier et al., 1989). IR spectroscopy can also be used successfully to study conformational changes during B→A and B→Z transitions (Adam et al., 1986; Pilet & Brahms, 1973; Taboury et al., 1985; Taillandier et al., 1989; Taillandier & Liquier, 1992) and DNA denaturation (Banyay et al., 2003; Lee et al., 2004). The IR spectra of DNA show many characteristic bands, which are sensitive to denaturation, dehydration and conformational transition. Table 4 shows the main IR absorption bands observed during the melting of DNA and transformation between B and A (or Z) forms. IR also allows single-stranded, double-stranded and triple-stranded chains of DNA to be distinguished (Banyay et al., 2003; Taillandier & Liquier, 1992). In the literature there are plenty of data on the conformational changes induced by pH or temperature changes (Lee et al., 2004; Tajmir-Riahi et al., 1995), dehydration (Falk et al., 1963; Lee et al., 2004) and interaction with metal ions such as Mn^{2+}, Co^{2+}, Ni^{2+}, Cu^{2+}, Cd^{2+}, Mg^{2+} and Pt^{2+} (Hackl et al., 2005; Matsui et al., 2009). IR spectroscopy is also a powerful technique in investigating the interaction of DNA with drugs (Taillandier & Liquier, 1992).

The IR spectrum can be divided into four characteristic spectral ranges. Absorbed in the range 1800-1500 cm^{-1} are bands related to the C=O, C=N, C=C and N-H stretching vibrations of bases. These bands are sensitive to changes in the base stacking and base pairing interactions. Bands occurring in the interval 1500-1250 cm^{-1} assigned to vibrations of the bases and base-sugar connections are strongly related to the conformational changes of the backbone chain and glycosidic bond rotation. The range 1250-1000 cm^{-1} involves sugar-phosphate vibrations, such as PO_2^- symmetric and asymmetric stretching vibrations and C-O stretching vibrations. These vibrations show high sensitivity to conformational changes in the backbone. The range 1000-800 cm^{-1} is characteristic for bands associated with vibrations of sugars which correlate with the various nucleic acid sugar puckering modes (C2'-endo and C3'-endo) (Adam et al., 1986; Banyay et al., 2003; Lee et al., 2004; Parker, 1983; Pevsner & Diem, 2003; Taillandier et al., 1989; Taillandier & Liquier, 1992).

It is worth mentioning that IR spectroscopy applied to nucleic acids gives structural information comparable to that obtained from X-ray crystallography or high resolution NMR. In addition, this method compared to the aforementioned techniques allows examination of the samples in various states.

B form	Bands observed for melting	Bands characteristic for B→A transition	Bands characteristic for B→Z transition	Assignments*
1715	-1690	1708	1690	ν(C=O), ν(C=C), ν(C=N), β(N-H)
1664	-1649	1664	1664	
1610	-1607	1605	1610	
			1433	dA syn
1425	-1410			dC2′-endo
		1418	1408	dC3′-endo
1375	+1362	1375		d purine/anti
			1355	d purine/syn
1292	disappears			ν(C4NH$_2$) of C
1280	disappears	1275		β(CN3H) of dT
			1265	dC, dG
1225	-1241	1240	1212	$\nu_{as}(PO_2^-)$
		1188		ν(C-O)b
1088	-1096	1088	1085, 1060	$\nu_s(PO_2^-)$
1052	+1069	1052		ν(C-O)d
970	-957	975, 970, 953	969, 951, 925	ν(C-C)b
894	-883	899, 877, 864	928	δd
840	-819	807	838	ν(O-P-O)b

*Abbreviations: ν, stretching; β, in-plane bending; δ, in-plane bending (ring); s, symmetrical; as, asymmetrical; dA, deoxyadenosine; dC, deoxycytidine; dG, deoxyguanosine; dT, thymidine; d, deoxyribose; b, backbone.

Table 4. Changes in the position of IR bands observed for melting of DNA, B→A and B→Z transitions. A plus (or minus) sign indicates a band which gained (or lost) appreciable intensity during melting.

2.3.2 Raman spectroscopy

Raman spectroscopy allows study of the structure of individual groups of atoms and provides information on the conformational changes taking place in macromolecules. Moreover, it is possible to monitor the denaturing processes (transition from ordered double stranded to a disordered single-stranded helix) and the B→A and B→Z conformational changes (Duguid et al., 1996; Erfurth & Peticolas, 1975; Prescott et al., 1984; Taillandier et al., 1989). Collected in Table 5 are the main Raman lines observed during the melting process and the B→A (Z) transitions. This technique also enables examination of the structural changes of DNA caused by radiation (Synytsya et al., 2007), temperature and pH change (Duguid et al., 1996; Erfurth & Peticolas, 1975; O'Connor et al., 1982) and the addition of metal ions or organic compounds (Duguid et al., 1993; Langlais et al., 1990; Martin et al., 1978; Martin et al., 1982).

The Raman spectrum can be divided into characteristic spectral regions. The dominated band in the range 1800-1600 cm^{-1} at 1668 cm^{-1} is assigned to coupled C=O stretching and N-H deformation modes of dT, dG and dC, which is very sensitive to the denaturation process. Located in the interval 1600-1200 cm^{-1} are bands associated with purine and pyrimidine ring vibrations. The bands are shaped by conformational transition and melting

process. In addition, they are perturbed by metal binding at ring sites and are sensitive indicators of electronic structure changes of the ring.

B form	Bands observed for melting	Bands characteristic for B→A transition	Bands characteristic for B→Z transition	Assignments*
1688	+1654, +1684	1688		ν(C=O), δ(NH2) of dT, dG, dC
1610	+1597	1603		dC
1578	+1572, -1582	1574	1577	dG, dA
1534	+1528	1533		dC
1511	+1504	1512	1521	dA, dC
1489	+1481, -1494	1483	1491	dG, dA
1421	+1412			d purine/syn
		1396		$d(CH_2\ \delta)$, dG
1376	+1365, -1381	1374	1362	dT, dA, dG
1339	+1324, -1343	1336	disappears	dA, dG
1320	+1320	1322		dG
			1314	d purine/syn
1304	+1308	1301		dA
1292	+1289		1292	dC
1257	+1257		1257	dC, dA
1238	+1238	1243	1238	dT
1218	+1218	1209	1220	dT
1186	+1183	1186	1186	dT, dC
1142	disappears	1145		ν(C-C)
1094	-1094	1099	1094	$\nu_s(PO_2^-)$
1054	+1060		1051	ν(C-O)
895	+872			d
835	-828	806	810	ν(O-P-O)
781	+773, -792		746	dC
750	+738	748	748	dT
729	+725	727	715	dA
		704		d
682	-682	682		dG C2′-endo/anti
			625	dG C3′-endo/syn

*Abbreviations: ν, stretching mode; δ, deformation mode; s, symmetrical; dA, deoxyadenosine; dC, deoxycytidine; dG, deoxyguanosine; dT, thymidine; d, deoxyribose; b, backbone.

Table 5. Changes in the position of IR bands observed for melting of DNA, B*A and B*Z transitions. Plus (or minus) sign indicates that the band has gained (or lost) appreciable intensity as a result of DNA melting

The symmetric PO_2^- band near 1092 cm^{-1} is correlated with changes in the electrostatic environment of the phosphate group. The bands in the range 1100-800 cm^{-1} characterize the backbone geometry and secondary structure. The region 800-600 cm^{-1} includes bands which are sensitive to nucleoside conformation. The transition near 750 cm^{-1} is assigned to C2'-endo/anti conformers of thymidine (Duguid et al., 1993; Erfurth & Peticolas, 1975; Prescott et al., 1984; Taillandier et al, 1989).
Raman spectra of nucleic acids in aqueous solution are not perturbed by water absorption, thus Raman spectroscopy can be used successfully to study both solids and aqueous solutions of DNA.

2.4 The primary and secondary action of Near Infrared Radiation on biological materials. Spectrophotometric study

2.4.1 Introduction

Phototherapy is one of the oldest therapeutic methods; initially known as solar therapy, later light therapy and low power laser therapy. Light therapy has been used for more than forty years to promote healing, reduce pain and inflammation and prevent tissue death. Light irradiation as a local phototherapeutic modality is characterized by its ability to induce non-thermic, nondestructive photobiological processes in cells and tissues. A variety of studies both *in vivo* and *in vitro* have shown that light irradiation has a significant influence on cell functional state. The response of light action is biphasic following irradiation both *in vitro* and *in vivo*. The so-called Arndt-Schultz curve of energy dose versus the response reveals that low doses of energy stimulate cell and tissue processes, while high energy doses reverse the stimulation and lead to inhibition.
Results of experiments *in vitro* and *in vivo* on isolated cells as well as on animals and humans are ambiguous. Despite many investigations on the subject, the therapy remains controversial largely due to uncertainties about the fundamental molecular and cellular mechanisms responsible for transducing signals from the photons incident on the cells to the biological effects that take place in the tissues illuminated. Different explanations based on light absorption by primary endogenous chromophores (mitochondrial enzymes, cytochromes, flavins and porphyrins) have been proposed to describe the biological effects of light. However, a precise theory concerning the therapeutic effects of light biostimulation has not been developed.
NIR radiation is widespread in medicine, both in therapy and diagnostics. It is recognized that NIR light is used to accelerate wound healing processes, reduce inflammations, support central nervous system regeneration, promote vascular and lymphatic microcirculation, stimulate the immune system and reduce and control pain (Eells et al., 2004; Posten et al., 2005; Sieron et al., 1994). Between 600 and 1200 nm is the so-called "therapeutic window" used in phototherapy. Radiation from this region is absorbed mainly by several tissue components, including water, glucose, hemoglobin, lipids, amino acids, proteins and nucleic acids (Olsztynska-Janus et al., 2008).
The effect of NIR radiation on biological systems was investigated using the example of erythrocytes and liposomes (Chludzińska et al., 2005; Komorowska et al., 2002a; Komorowska et al., 2002b; Komorowska & Czyżewska, 1997). Radiation in this range reduces the ability of cells and liposomes to aggregate. Exposure to NIR decreases the rate of hemolysis with increasing resistance of the membranes, which in turn is associated with increased flexibility and mechanical strength of erythrocyte membranes. NIR radiation protects them from oxidative stress, and thus affects the stabilization of the aging process of erythrocytes.

We attempted to resolve the molecular mechanism of the photochemical and therapeutic action of light in the NIR region *in vivo* and *in vitro* on the basis of results from spectrophotometric study of such molecules as amino acids, proteins and DNA.

2.4.2 NIR action on the amino acid phenylalanine

In order to explain the process undergone following exposure to NIR, a simple object was studied, in this case phenylalanine amino acid (Olsztynska-Janus et al., 2009; Olsztynska-Janus et al., 2008). The FTIR-ATR spectra of L-phenylalanine aqueous solutions were measured between 4000 and 700 cm^{-1}. Quantum chemical calculations, performed in parallel, made it possible to propose the primary and secondary process induced by the NIR irradiation. According to the results obtained, the interaction between two identical amino acids involves hydrogen bonding –C=O···HOOC–, which leads to cyclic dimers analogous to those formed by carboxylic acids (Olsztynska et al., 2003). The dimer formation is preceded by conformational changes of the amino acid. The greatest possible is the *trans/cis* transition. As a consequence of dimer formation, the p*K*a values of the amino acid can be shifted (Figure 3, Table 6) (Olsztynska et al., 2006b).

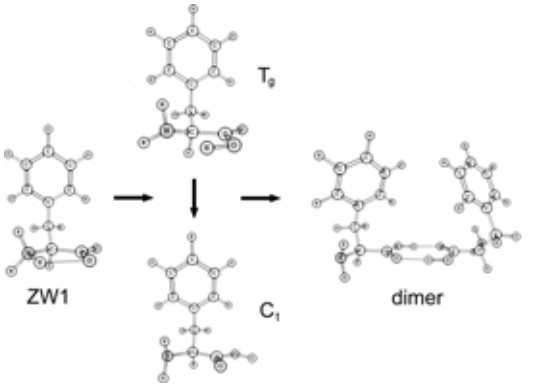

Fig. 3. NIR effect on conformational changes of phenylalanine zwitterion (ZW) due to *trans/cis* isomerization (T_g/C_t), dimer formation and shifts of p*K*a values (see Table 6).

	Dark Phe	NIR Phe	ΔpK_a
pK_1	2.31	2.79	+0.48
pK_2	9.28	8.66	–0.62

Table 6. p*K*a values of phenylalanine before (dark) and after NIR irradiation. Δ p*K*a is the difference between p*K*a ($pKa_{Phe(NIR)} - pKa_{Phe(Dark)}$).

2.4.3 NIR action on DNA

2.4.3.1 Mathematical techniques used to study changes in spectroscopic data

2.4.3.1a Principal components analysis (PCA)

According to Brereton, "PCA is probably the most widespread multivariate chemometric technique … that most significantly changed the chemist's view of data analysis." (Brereton,

2003). In the literature there are many examples of application of PCA as an efficient tool supporting medical diagnosis, where the DNA bands have important contributions (Ly et al., 2009; Owen et al., 2006; Petrich, 2001; Wood et al., 2000).
PCA is an abstract transformation of the original data X matrix with m rows and n columns, and with each wavenumber (variable) being a column and each spectrum (sample) a row, into a sum of k $t_1$and p_1 vectors.

$$X = t_1 p_1^T + t_2 p_2^T + ... + t_k p_k^T + E \quad (1)$$

The t_1 vectors are known as scores and contain information on how the samples relate to each other. The p_1 vectors are known as loadings and contain information on how the variables relate to each other. The t_1, p_1 pair captures the greatest amount of variation in the data, where as each subsequent pair captures the greatest possible amount of variance remaining after subtracting $t_1 p_1^T$ from X. The number of principal components (PCs) that can adequately describe variations in the raw data X is equal k. In general, the raw data can be adequately described using far fewer factors than original variables. The reduction of the large amount of original data to a much smaller, more manageable dataset is a major advantage of PCA. This method provides great potential for the visualization of relations between samples and variables against PCs. Score plots allow many different questions on the relationships between objects to be answered. Loading plots provide detailed information about which wavenumbers are most associated with which object. PCA also provides an answer to the question of grouping samples into clusters. Measurements of distances between samples allow the number of clusters and similarity of objects inside the clusters to be determined.

2.4.3.1b Two-dimensional correlation spectroscopy

To the question "Vibrational spectroscopy: a 'vanishing' discipline? Meier answers that "… compared to the past, a shift in applications has taken place, bringing new opportunities. This is partly due to the introduction of new features, including … 2D correlation spectroscopy (Meier, 2005). Specific applications of vibrational spectroscopy in biomedical engineering can be also enhanced substantially by application of the 2D correlation technique, which will be shown in the next section. A detailed introduction to the subject of 2D correlation spectroscopy is beyond scope of this work and therefore is kept to a minimum. Readers interested in this technique are referred to the monograph published in 2004 (Noda & Ozaki, 2004) which remains as the most authoritative reference source in this field. Recently, to mark the Fifth International Symposium on Two-Dimensional Correlation Spectroscopy (2DCOS-5) held in Wrocław, Poland in August 2009, a comprehensive review on research aided by 2D correlation spectroscopy was compiled by Noda (Noda, 2010). It covers the period between 2007 and 2009, with many different examples discussed, also analysis of which was substantially improved thanks to application of the 2DCOS method.
Generally speaking, the 2DCOS is recognized as a very efficient procedure for enhancement of the spectral resolution of a broad absorption envelope that hides bands assigned to vibrations having a different response to a perturbation applied. The 2DCOS calculations begin with arrangement of the measured data into the X matrix. In the majority of cases the 2D calculations are preceded by subtraction of the reference spectrum of the system from the raw-pretreated data. The result of the subtraction is called the dynamic spectrum ($\tilde{Y}$) because it presents the response of the system perturbed to the perturbation applied. If an

averaged spectrum is chosen as the subtrahend, the dynamic spectra are identical to the mean-centered spectra and synchronous 2D correlation intensities ($\Phi(v_1, v_2)$) have the same sense as covariance matrix ($\mathrm{cov}(\tilde{\mathrm{Y}})$).

$$\Phi(v_1, v_2) = \frac{1}{m-1}\tilde{\mathrm{Y}}(v_1)^T \times \tilde{\mathrm{Y}}(v_2) = \mathrm{cov}(\sim \tilde{\mathrm{Y}}) \tag{2}$$

The discrete form of an asynchronous 2D spectrum $\Psi(v_1, v_2)$ is obtained by multiplying the data matrix $\tilde{\mathrm{Y}}$ by the orthogonal counterpart of $\tilde{\mathrm{Y}}$, obtained using the Hilbert transformation (N).

$$\Psi(v_1, v_2) = \frac{1}{m-1}\tilde{\mathrm{Y}}(v_1)^T \times N \times \tilde{\mathrm{Y}}(v_2) \tag{3}$$

Much useful information is available from synchronous and asynchronous spectra analyzed according to the guidelines popularly known as Noda's rules (Noda & Ozaki, 2004). Some of the most important information provided is the sequential order of events observed using the spectroscopic technique along the external perturbation. It finds excellent application in many studies, allowing, for example, the evolution of the unfolding mechanism of polypeptides (Ashton et al., 2006) and proteins to be investigated (Czarnik-Matusewicz et al., 2009). Whenever the correlated wavenumbers come from different spectral ranges the method is known as a heterospectral 2D correlation. Such modification of 2D correlation spectroscopy enhances the content and quality of spectral information in relation to that obtained with 2D homospectral correlation (Jung et al., 2000).

2.4.3.1c Combined PCA-2DCOS analysis of the DNA films

Our previous research performed for aqueous solutions of herring sperm DNA irradiated by NIR light for periods of 5, 10 and 20 minutes revealed distinct differences for melting profiles obtained from UV and FTIR-ATR measurements (Szymborska-Małek et al., 2009a, b). Most probably, properties of the water comprising a shell around DNA are modified during the irradiation in a manner dependent on the dose of NIR light exposure. According to results already obtained, the NIR-reshaped hydration shell leads to liposomes being more able to agglomerate (Komorowska et al., 2006) and to aggregation of L-phenylalanine (Olsztynska-Janus et al., 2009). The aim of the present research is an analysis of the phenomenon for DNA with limited water content. The measurements were therefore performed for thin film samples obtained from solutions of DNA following water evaporation to a constant level. The effect of the NIR radiation is hard to discuss in detail without application of some pattern recognition method due to minute absorbance changes caused by temperature increase, as shown in Figure 4. The profiles were so common across the four sets of data that it was not possible to distinguish differences between them by way of ordinary analysis.

The spectra presented above are results of pretreatments performed in the following order:

- denoising by means of the coif-5 mother wavelet with a five-level decomposition and soft thresholding criterion;
- the second order baseline correction at the same three anchor points;
- the offset at 1810 cm^{-1};
- normalization over the integral area calculated in the range analyzed, i.e. 1810-867 cm^{-1}.

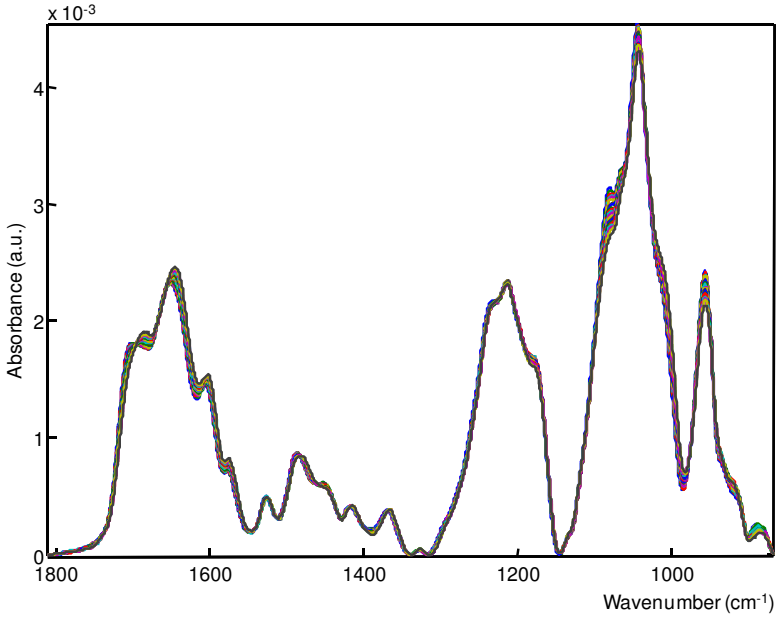

Fig. 4. FTIR-ATR temperature-dependent spectra recorded for DNA film obtained from solution unexposed to NIR radiation. Measurement was performed within the temperature range 25-90°C (for colour see www.intechweb.org).

It is very important to apply the same procedures of pretreatment to all spectra subjected to PCA and 2DCOS calculations, which was strictly respected in the research presented.
Applying PCA, the pattern between samples arising independently from temperature and NIR radiation can be successfully investigated. The bands sensitive to effects of base pairing and base stacking which are strongly overlapped and difficult to assign due to the wide-type of measured DNA can be resolved substantially by 2DCOS analysis.
Here the main concepts of PCA and 2DCOS will be illustrated by the analysis of the four sets of the FTIR-ATR temperature-dependent spectra collected for the films of DNA samples obtained from DNA-buffer solutions irradiated for 5, 10 and 20 minutes by NIR light. The non-irradiated solution, treated as the control, was also subjected to the same temperature studies. For clarity the notations 5^{NIR}, 10^{NIR}, 20^{NIR} and 0^{NIR} will be used, respectively, for the samples. The spectral range selected for the PCA analysis is composed of many strongly overlapped bands attributed to different moieties of the DNA film which undergo very small variations with temperature increase. The primary purpose of the research has been to provide information on the influence of NIR radiation on DNA structure. In particular, the research was conducted for film samples where there is no absorption from water which very strongly overlaps with that originating from vibrations of different nucleobases. The bands are extremely sensitive to base stacking and base pairing interactions and are changed substantially during the thermal denaturation process. One of the main advantages of using PCA is its ability to convert the multivariate data to a simple graphical presentation. Among the many ways of visualizing PCs one of the simplest is that of the score of one PC against the other.

Figure 5 illustrates the PC plot for the first two PCs, which together capture 86% of the spectral variance for the matrix comprising all of the four sets of data. The first PC captures the largest amount of variations in the data set, i.e. 73%, which are independent of the 13% of variations captured by the second PC. For the system studied, the two principal components adequately describe all of the variation in the spectra measured induced by both temperature changes and NIR radiation. Each circle in the loading plot represents the location of a spectrum projected into the plane defined by the pairs of first two principal component axes. The circles are differently colored to assist in distinguishing the samples exposed to NIR radiation at different periods of time. The loading plot very clearly show that the first PC captures the major absorbance changes induced by temperature increase, whereas the second PC captures the minor absorbance changes caused by NIR radiation. They are almost 6 times smaller than those induced by temperature.

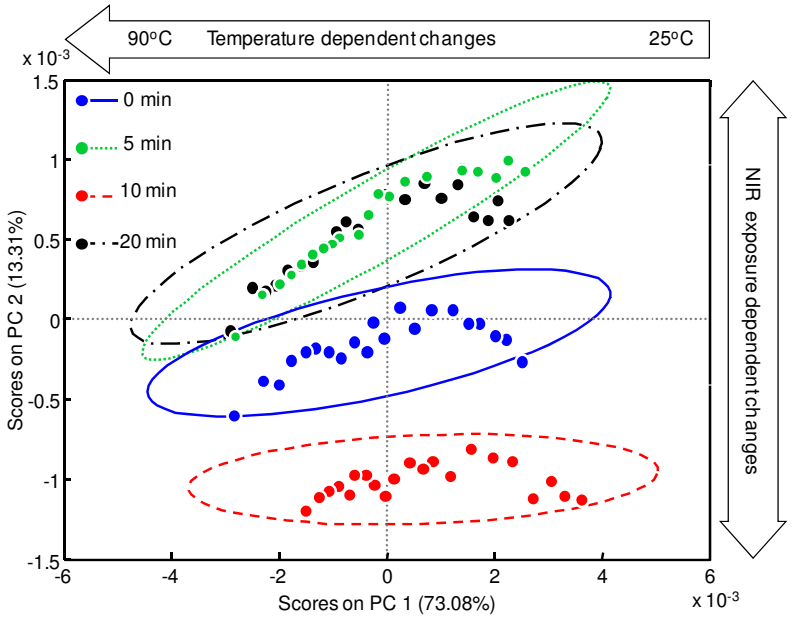

Fig. 5. Score plot of the spectra for the four systems combined into one matrix for the first two PCs (for colour see www.intechweb.org).

Analyzing the distribution of the samples against the first PC makes it easily noticeable that the 5^{NIR}, 20^{NIR} and 0^{NIR} for temperatures between 25°C and 62°C are characterized by positive scores, while negative scores relate to measurements performed at temperatures above 62°C. For the 10^{NIR} sample the border between positive and negative scores is shifted from 62 to 68°C. Distribution of scores against PC1 reveals that all samples undergo a very similar process of structural change due to temperature increase, excepting the fact that the extent of the change induced for the 10^{NIR} sample is smaller than for the others.

The second PC that captures the remaining changes, not described by PC1, correlates with the period of NIR radiation. According to the analysis of the distribution of samples against the PC2, i.e. along the vertical axis, the whole data set should be divided into three clusters. The 10^{NIR} sample has more negative scores on PC2, the 0^{NIR} sample is almost uncorrelated

with the period of NIR radiation, whereas the 5^{NIR} and 20^{NIR} are characterized by positive scores. Moreover, the slopes of the clusters reveal that the influence of NIR radiation on the absorbance changes decreases with temperature elevation, except in the case of the 10^{NIR} sample.

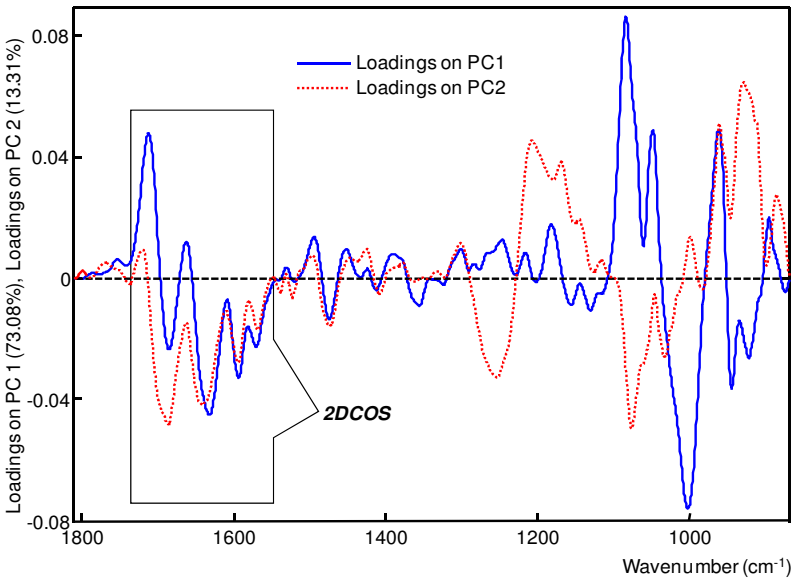

Fig. 6. Loading plot of the spectra for the four systems combined into one matrix for PC1 (solid line) and PC2 (dotted line). The grey box contains a marked range selected for 2DCOS calculations (for colour see www.intechweb.org).

The next step of PCA always involves examination of the loading plot to see which variables fulfil the conditions described by subsequent scores. Analysis of the loading plot shown in Figure 6 analyzed in the context of PC1 enable discrimination between absorbance changes at the two stages of heating resolved by scores values. This allows it to be determined that at the initial steps of heating, beginning at 25°C, the more active bands are those at 1081, 1711, 1047 and 959 cm^{-1}. According to the literature data (Banyay et al., 2003; Parker, 1983;), the first is attributed to the $\nu_s(PO_2^-)$ vibration and is sensitive to the changes in hydration pattern around the phosphate groups, whereas that at 1711 cm^{-1} relates to changes in base pairing as it arises from in-plane stretching modes of the C=O groups of paired bases. The band at 1047 cm^{-1} also reflects changes in hydration of backbone as it is mainly attributed to C-O skeletal vibrations of ribose. The last band at 959 cm^{-1} is assigned to ribose-phosphate skeletal motions. All of the changes indicate that a temperature increase from 25°C to 60°C causes changes in backbone configuration and in base pairing interaction for the low hydrated films. For higher temperatures it is mainly changes at 1000, 1632, 942, and 919 cm^{-1} which are manifested on the loadings distribution against PC1. All of the bands, except that at 1632 cm^{-1}, are characteristic of ribose-phosphate main chain vibration. The other arises from combined C=N and C=C vibration of base residues. The separation of the bands into the two groups according to sign of loadings reveals the separate character of conformational changes in the DNA dehydrated film at lower and higher temperatures. The phosphate groups generally very sensitive to

changes in hydration properties also in dehydrated conditions undergo perturbation accompanied by base-pairing interaction changes. This process evolves below 60°C, whereas above the temperature another begins, embracing the phosphodiester moieties and the aromatic rings of bases. An important fact is that the band assigned to the $\nu_{as}(PO_2^-)$ vibration is almost totally insensitive to temperature changes.

The loading plot reflects very clearly the differences in response of the symmetric and antisymmetric stretching vibrations for the PO_2^- group with the temperature increase and the NIR radiation effect. The $\nu_{as}(PO_2^-)$ band is sensitive to both varying hydration and orientation of the phosphate group, whereas the $\nu_s(PO_2^-)$ is sensitive to orientation only (Parker, 1983) and changes in the dielectric environment around the phosphate group which are responsible more for its intensity variations than its shift (Pevsner & Diem, 2003). As a consequence of their different sensitivity to hydration, the $\nu_{as}(PO_2^-)$ is a characteristic marker for backbone conformational changes between B- and A-form, as the B-A transition is strictly correlated with deficiency of water in the hydration sphere of the phosphate groups. For the $\nu_s(PO_2^-)$ its insensitivity to hydration involves a lack of influence on its position by the B-A transition, but its intensity could be influenced by subtle changes in the local polarity.

Examination of the loading plot against the second PC2 allows bands for which absorbance is correlated with dose of NIR radiation to be selected. For the 10^{NIR} sample most characteristic are the two stretching bands arising from vibration of the PO_2^- group and bands assigned to the in-plane base vibrations. Moreover, from combined observation of loadings for PC2 against PC1 it can be stated that in the case of the $\nu_s(PO_2^-)$ vibrations at 1074 cm^{-1} the NIR effect is better distinguished at lower temperatures, whereas for the $\nu_{as}(PO_2^-)$ vibration at 1253 cm^{-1} this effect is manifested at higher temperatures. This means that in the case of the 10^{NIR} sample that due to the NIR radiation both on the hydrational, orientational properties of the phosphate groups as well as the local dielectric constant in vicinity of PO_2^- are modified. The absorbance changes at 1686, 1641, 1593 and 1569 cm^{-1} which arise from the in-plane base vibrations dominate at temperatures above 70°C. This means that for the thin film samples the NIR-dependent alternations in base pairing and base stacking interactions, more strongly manifested at higher temperatures, are preceded by variations in the NIR-modified hydration layer which is sensitive to temperature changes at lower range. For the 5^{NIR} and 20^{NIR} samples the phosphate symmetric and in-plane base vibrations are not affected by NIR. However, the band at 1207 cm^{-1}, attributed to the $\nu_{as}(PO_2^-)$ vibration, is 46 cm^{-1} red shifted relative to the band at 1253 cm^{-1} for the 10^{NIR} sample, which indicates better hydration of the phosphate groups for 5^{NIR} and 20^{NIR}. The band at 1168 cm^{-1}, as a marker of A-form, reveals a different degree of B-A transition for the two groups of samples. Also the bands at 958 and 927 cm^{-1} sensitive to the changes in the B-A transition are well resolved in the loadings plotted against PC2. Based on the PCA results presented, we are able to suggest that due to NIR radiation mainly hydration pattern around the phosphate groups is modified and the extent of the changes can be modulated by the period of the NIR radiation.

The advantages arising from using 2DCOS in analysis of spectra composed from many overlapped bands will be presented for a selected range of 1850-1550 cm^{-1} contributed by several in-plane base vibrations. The changes in base-stacking and helical stability are evidenced by the complex intensity changes of their bands. Also the synchronous spectra in Figure 7 obtained for the four data sets confirm that the changes developed in the 1850-1550 cm^{-1} range for the 10^{NIR} sample (see Fig. 7C) have a pattern different from those for the other three systems.

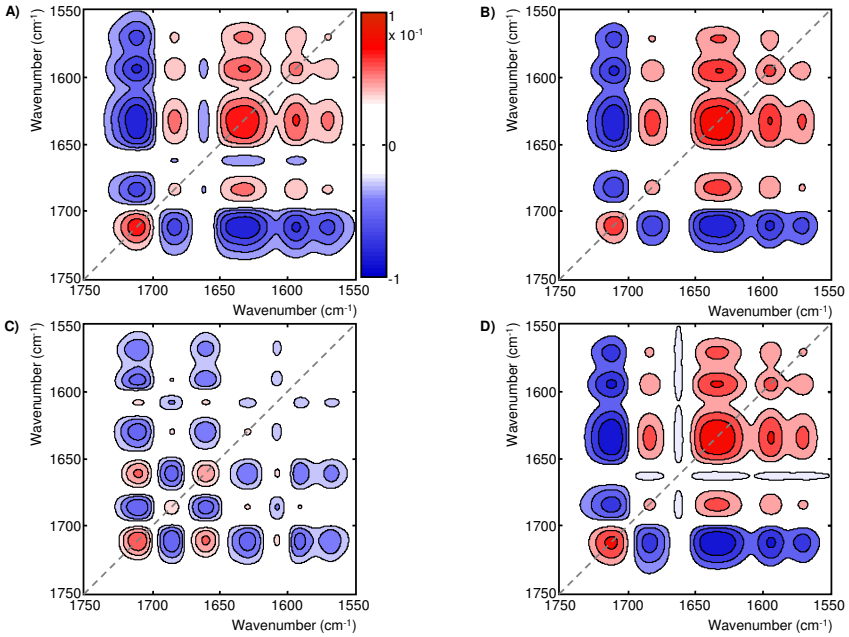

Fig. 7. Synchronous 2D FTIR-ATR correlation spectra obtained from the temperature-perturbed measurements for the 0^{NIR} (A), 5^{NIR} (B), 10^{NIR} (C) and 20^{NIR} (D) systems (for colour see www.intechweb.org).

For the synchronous map an important feature is the sign of the ($\Phi(v_1,v_2)$) peaks which represents the simultaneous or coincidental changes of two separate spectral intensity variations measured at v_1 and v_2 during the temperature changes from 25 to 90°C. Positive cross peaks, i.e. peaks outside the diagonal, indicate that their correlated intensities are either increasing or decreasing with the function of the temperature increase, whereas negative peaks indicate that the correlated changes are in opposite directions. The positions and signs of the ($\Phi(v_1,v_2)$) peaks from Figures 7A, B and D allow identification of only one peak at 1712 cm^{-1}, the intensity of which decreased with temperature, and four peaks at 1684, 1634, 1594 and 1570 cm^{-1}, the intensity of which increased with temperature elevation. In the literature, there is a large diversity in assignments of the bands for the ν(C=O) vibrations. According to the most comprehensive review of this topic available to date (Banyay et al., 2003), in the range of the ν(C=O) vibrations, a double strand (*ds*) to single strand (*ss*) transition results in a decrease in intensity of the bands at higher frequencies with a concomitant increase in intensity of the bands at lower frequencies. In addition, bands arising from the in-plane stretching modes of the C=C and C=N groups of bases and the NH_2 scissoring vibrations, located below 1650 cm^{-1}, gain in intensity at the *ds* to *ss* transition. In accordance with these facts are the changes developed for the 0^{NIR} (Fig. 7A), 5^{NIR} (Fig. 7B) and 20^{NIR} (Fig. 7D) systems, whereas for the 10^{NIR} system (Fig. 7C) the 2D synchronous map has an additional two peaks of different sign. The peak at 1660 cm^{-1} arising from the ν(C=O) vibration loses intensity with temperature increase, while the peak at 1607 cm^{-1} is amplified.

Figure 8 presents the power spectra extracted from the synchronous maps. The peaks are located at diagonal positions and their intensity is a measure of the overall extent of spectral intensity variations due to temperature elevation from 25 to 90°C. As Figure 8 shows, for the 10^{NIR} system the in-plane ring vibrations from the C=C and C=N are less perturbed than the C=O vibrations during the heating process. This could mean that for the system irradiated for 10 minutes during heating the changes in base pairing predominate over the changes in base stacking. For the other system the two kinds of interaction change to a similar extent with temperature increase.

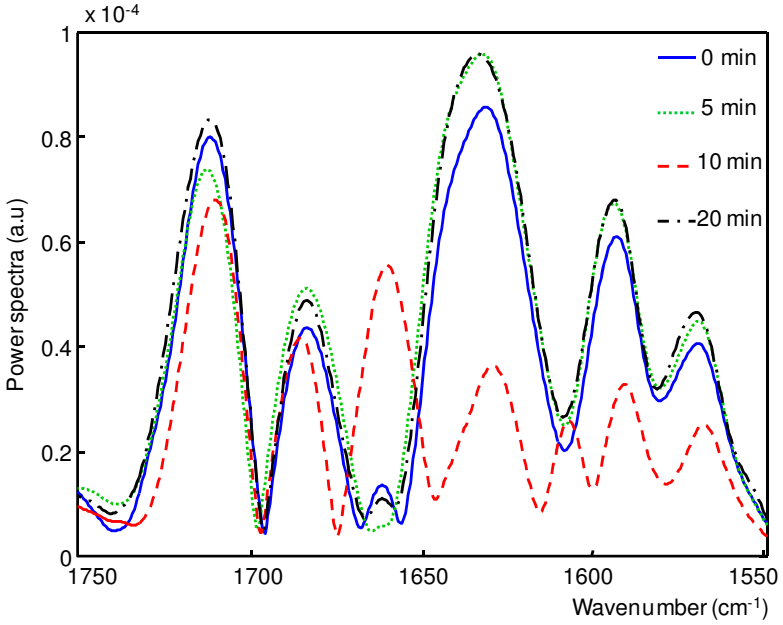

Fig. 8. The power spectra extracted from the synchronous maps (for colour see www.intechweb.org).

The pattern of peaks at the asynchronous spectra in Figure 9 confirms the different behavior of the 10^{NIR} system during the temperature destruction of the *ds* structure. The asynchronous peaks develop at frequencies at which the intensities are changing in an uncorrelated manner. Their sign provides useful information on the sequential order of the processes developed in the course of the temperature changes from 25 to 90°C which are detected by FTIR-ATR spectroscopy. For the 0^{NIR} system most asynchronous are the peaks that combine different ν(C=O) vibrations and the ν(C=O) vibrations with the in-ring. This same is true for the 5^{NIR} and 20^{NIR} systems. For the 10^{NIR} system the bands attributed to the ν(C=O) vibrations are asynchronously correlated only with the in-plane ring. This confirms that the base pairing and base stacking interactions are differently modified by NIR radiation. For all of the systems the changes in the base pairing interaction are ahead of the changes in base stacking. These findings are in good agreement with the available scenarios for the melting of *ds*DNA where pairing and stacking are treated as separate, non-cooperative processes (Gonzales et al., 2009).

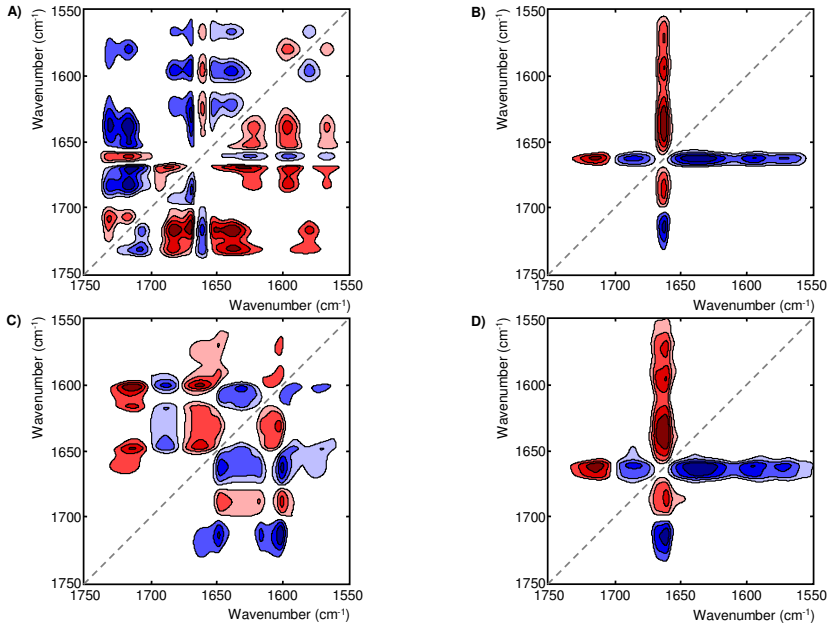

Fig. 9. Asynchronous 2D FTIR-ATR correlation spectra obtained from the temperature-perturbed measurements for the 0^{NIR} (A), 5^{NIR} (B), 10^{NIR} (C) and 20^{NIR} (D) systems (for colour see www.intechweb.org).

2.4.4 Stress/strain measurements in soft matters by Raman spectroscopy

Raman spectroscopy is a very powerful tool for the study of stress-induced molecular changes in natural and synthetic polymers (Amer, 2009; Koening, 2001). The application of stress leads to changes in interatomic distances and consequently shifts the positions of the bands. Such effects have been observed in silk, wool and collagen fibre analysis (Church et al., 1998; Colomban et al., 2008; Sirichaisit et al., 2000; Wang et al., 2000).

For unstrained wool fibres, the maximum of amide I band was found at 1652 cm^{-1} (typical for α helical proteins) and shifted to 1672 cm^{-1} (β-pleated sheet conformation) in the spectrum for stretched fibres. An intensity of peak observed at 1239 cm^{-1} (amide III, β-pleated sheet structure) increases during stretching, which confirms information obtained from amide I band analysis (Church et al., 1998). The α-β transition caused by stretching silk fibres was also reported (Colomban et al., 2008). The significant, almost linear, stress-induced shift was observed for ν(C-C) band at 1095 cm^{-1} in the silk Raman spectrum. Elongation of polypeptide backbone occurs when the fibre is stretched (Sirichaisit et al., 2000). Deformation of protein backbone was also noticed for rat tail collagen (Wang et al., 2000).

The Raman spectrum of soft tissues is dominated by the structural protein bands: $\delta(CH_2, CH_3)$ (~1450 cm^{-1}), $\nu(C_\alpha\text{-}C)$ (~940 cm^{-1}) and amide bands. Amide I and III bands for triple-helical collagen structure are observed near 1668 and 1248 cm^{-1}, respectively. Elastin exhibits bands in positions typical for unordered proteins, i.e. at 1662 cm^{-1} and 1250 cm^{-1}. Apart from protein, in skin and aorta spectra, weaker intensity lipid bands (1100-1150 cm^{-1}) are to be

seen. The tendon has a hierarchical structure and is composed of collagen molecules, fibrils, fibre bundles, fascicles and tendon units that run parallel to the tendon's long axis. The diameter of the fibril depends on species, age and location. Tendon also contains small amounts of elastin (~2%) (Penteado et al., 2006; Silver et al., 2003; Wang et al., 2000).

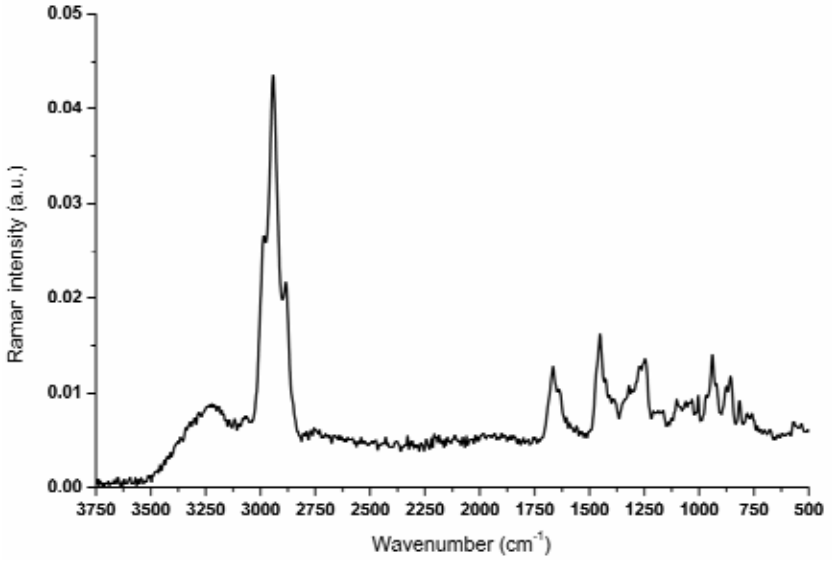

Fig. 10. Representative Raman spectrum of pig tail tendon.

Peak position (cm^{-1})	Assignments
3225	ν(NH), ν(OH)
2940	$\nu(CH_2)$
1666	ν(C=O), amide I, collagen, elastin
1451	$\delta(CH_2, CH_3)$
1266	ν(CN), δ(NH), amide III, non-polar triple helix of collagen
1248	ν(CN), δ(NH), amide III, polar triple helix of collagen, elastin
1004	ν(CC), phenylalanine
940	$\nu(C_\alpha\text{-}C)$, α-helix
922	ν(CC), proline
875	ν(CC), hydroxyproline
856	ν(CC), proline
815	ν(CC), protein backbone

Table 6. Major bands identified in tendon spectra (Gąsior-Głogowska et al., 2010).

The major peaks in tendon spectra, shown in Figure 10, are attributed to the proteins: $\nu(CH_2)$ (~2942 cm^{-1}), $\delta(CH_2, CH_3)$ (~1450 cm^{-1}), $\nu(C_\alpha\text{-}C)$ (~940 cm^{-1}) and amide bands, with maxima of 1666 cm^{-1} (amide I) and 1249 cm^{-1} (amide III). The amide I band in the unstrained tendon

spectrum is strongly asymmetric and its deconvolution allowed identification of few components within 1600-1700 cm^{-1}: collagen (1631 and 1666 cm^{-1}), hydrated water (1641 cm^{-1}), elastin (1653, 1675 and 1683 cm^{-1}) and aromatic amino acids (1606, 1617 and 1698 cm^{-1}). In the amide III region bands assigned to unordered (1248 cm^{-1}) and triple-helical (1266 cm^{-1}) collagen structure are observed. The weak shoulder of the amide III band at 1239 cm^{-1} is due to elastin. The bands near 875, 856 and 922 cm^{-1} can be assigned to ν(C-C) modes of amino acids characteristic for collagen, i.e. hydroxyproline and proline. The band near 1004 cm^{-1} is assigned to the phenyl ring breathing mode of phenylalanine. Table 6 lists the wavenumbers of the observed bands and their assignment (Dong et al., 2004; Gąsior-Głogowska et al., 2010; Penteado et al., 2006; Wang et al., 2000).

When a pig tail tendon sample is subjected to increased levels of macroscopic strain, noticeable changes in the position of amide III bands in several stages are noted as shown in Figure 11. The observed variations mean protein backbone alternation. A significant shift for C_{α}–C stretching vibrations at 940 cm^{-1} also took place.

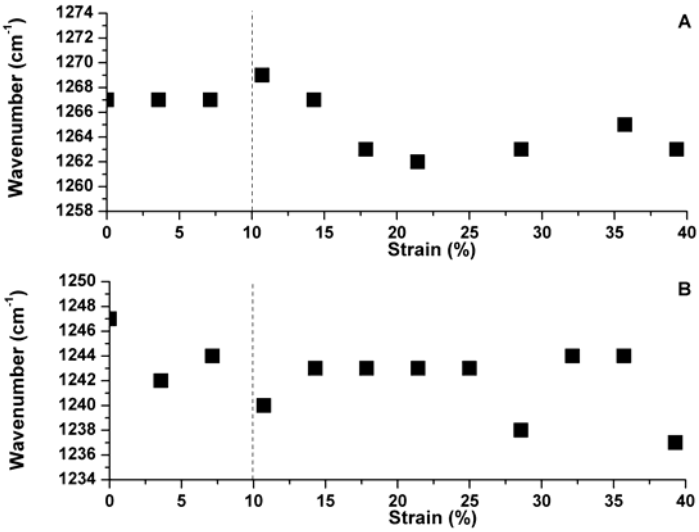

Fig. 11. Raman spectra of the tendon as a function of strain: A) proline-rich triple helix of collagen; B) proline-poor triple helix of collagen and elastin (Gąsior-Głogowska et al., 2010).

The amount and distribution of elastin and collagen fibres determine the mechanical properties of the soft tissues. Spectroscopic analysis shows differing tension thresholds for rich collagen material (ligaments, tendons) and tissues containing a high amount of elastin (blood vessel walls, skin). Moreover, the stress–strain plots and the Raman spectra recorded for the circumferentially and longitudinally oriented samples of aortic wall show significant differences (Hanuza et al., 2009).

3. Affiliation

This chapter is part of project "Wrovasc – Integrated Cardiovascular Centre", co-financed by the European Regional Development Fund, within Innovative Economy Operational Program, 2007-2013.

4. References

Adam, S.; Liquier, J.; Taboury, J.A. & Taillandier, E. (1986). Right- and left-handed helixes of poly[d(A-T)].cntdot.poly[d(A-T)] investigated by infrared spectroscopy. *Biochemistry*, Vol. 25, No. 11, 3220-3225.

Ahmed, A. & Tajmir-Riahi, H.A. (1993). Interaction of toxic metal ions Cd2+, Hg2+, and Pb2+ with light+harvesting proteins of chloroplast thzlakoid membranes. An FTIR spectroscopic study. *J. Inorg. Biochem.*, Vol. 50, No. 4, 235-243.

Amer, M.S. (2009). *Raman Spectroscopy for Soft Matter Applications,* John Wiley & Sons, Inc., ISBN 978-0-470-45383-4, Hoboken, New Jersey.

Amharref, N.; Beljebbar, A.; Dukic, S.; Venteo, L.; Schneider, L.; Pluot, M. & Manfait, M. (2007). Discriminating healthy from tumor and necrosis tissue in rat brain tissue samples by Raman spectral imaging. *Biochim. Biophys. Acta*, Vol. 1768, No. 10, 2605-2615.

Ashton, L.; Barron, L.D.; Czarnik-Matusewicz, B.; Hecht, L.; Hyde, J. & Blanch, E.W. (2006). Two-dimensional correlation analysis of Raman optical activity data on the α-helix-to-β-sheet transition in poly(L-lysine). *Mol. Phys.*, Vol. 104, No. 9, 1429– 445.

Banyay, M., Sarkar, M. & Gräslund, A. (2003). A library of IR bands of nucleic acids in solution. *Biophys. Chem.,* Vol. 104, No. 2, 477-488.

Barth, A. (2007). Infrared spectroscopy of proteins. *Biochim. Biophys. Acta*, Vol. 1767, No. 9, 1073-1101.

Bolton, B.A. & Scherer, J.R. (1989). Raman spectra and water absorption of bovine serum albumine. *J. Phys. Chem.*, Vol. 93, No. 22, 7635-7640.

Brereton, R.G. (2003). *Chemometrics: Data Analysis for the Laboratory and Chemical Plant,* Wiley, ISBN 0-471-48978-6, Chichester.

Byler, D.M. & Susi H. (1986). Examination of the secondary structure of proteins by deconvolved FTIR spectra. *Biopolymers*, Vol. 25, No. 3, 469-487.

Cai, S. & Singh B.R. (2004). A distinct utility of the amide III infrared band for secondary structure estimation of aqueous protein solutions using partial least squares methods. *Biochemistry*, Vol. 43, No. 9, 2541-2549.

Cai, S. & Singh B.R. (1999). Identification of beta-turn and random coil amide III infrared bands for secondary structure estimation of proteins. *Biophys. Chem.*, Vol. 80, No. 1, 7-20.

Cambpell, M.K. & Farrell, S.O. (2009). Biochemistry, Brooks Cole; 6th edition, ISBN-13: 9780495390411, 1-36, 235-260, Belmont

Cao, X. & Fischer, G. (1999). New infrared spectra and the tautomeric studies of purine and αl-alanine with an innovative sampling technique. *Spectrochim. Acta A*, Vol. 55, No. 11, 2329-2342.

Chan, K.L.A.; Kazarian, S.G.; Mavraki, A. & Williams, D.R. (2005). Fourier transform infrared imaging of human hair with a high spatial resolution without the use of a synchrotron. *Appl. Spectrosc.*, Vol. 59, No. 2, 149-155.

Chludzińska, L.; Jarosławska, E. & Komorowska, M. (2005). Near-infrared radiation protects the red cell membrane against oxidation. *Blood Cells, Mol. Dis.*, Vol. 35, No. 1, 74-79.

Church, J.S., Corino, G.L.; Woodhead, A.L. (1998). The effect of stretching on wool fibres as monitored by FT-Raman spectroscopy. *J. Mol. Struct.*, Vol. 440 No. 1-3, 15-23.

Cieślik-Boczula, K.; Czarnik-Matusewicz, B.; Perevozkina, M.; Filarowski, A.; Boens, N.; De Borgraeve, W.M. & Koll, A. (2007). ATR-IR spectroscopic study of the structural changes in the hydraophobic region of an ICPAN/DPPC bilayers. *J. Mol. Struct.*, Vol. 878, No. 1-3, 162-168.

Colomban, P.; Dinh, H.M.; Riand, J.; Prinsloo, L.C. & Mauchamp, B. (2008). Nanomechanics of single silkworm and spider fibres: a Raman and micro-mechanical *in situ* study of the conformation change with stress. *J. Raman Spectrosc.*, Vol. 39, No. 12, 1749-1764.

Czarnik-Matusewicz, B., Kim, S.B. & Jung, Y.M. (2009). A Study of Urea-dependent Denaturation of β-Lactoglobulin by Principal Component Analysis and Two-dimensional Correlation Spectroscopy. *J. Phys. Chem. B.*, Vol. 113, No. 2, 559–566.

Damm, U.; Kondepati, V.R. & Heise, H.M. (2007). Continuous reagent-free bed-side monitoring of glucose in biofluids using infrared spectrometry and micro-dialysis. *Vib. Spectrosc.*, Vol. 43, No. 1, 184–192.

Dong, A., Huang P. & Caughey W.S. (1990). Protein Secondary Structures in Water from Second-Derivative Amide I Infrared Spectra. *Biochemistry*, Vol. 29, No. 13, 3303-3308.

Dong, R.; Yan, X.; Pang, X. & Liu, S. (2004). Temperature-depended Raman spectra of collagen and DNA, *Spectrochim. Acta Part A*, Vol. 60, No. 3, 557-561.

Dousseau, F. & Pézolet M. (1990). Determination of the Secondary Structure Content of Proteins in Aqueous Solutions from Their Amide I and Amide I1 Infrared Bands. Comparison between Classical and Partial Least-Squares Methods. *Biochemistry*, Vol. 29, No. 37, 8771-8779.

Duguid, J.G.; Bloomfield V.A.; Benevides, J.M. & Thomas Jr, G.J. (1993). Raman spectroscopy of DNA-metal complexes. I. Interactions and conformational effects of the divalent cations: Mg, Ca, Sr, Ba, Mn, Co, Ni, Cu, Pd, and Cd. *Biophys. J.*, Vol. 65, No. 5, 1916-1928.

Duguid, J.G.; Bloomfield V.A.; Benevides, J.M. & Thomas Jr, G.J. (1996). DNA melting investigated by differential scanning calorimetry and Raman spectroscopy. *Biophys. J.*, Vol. 71, 3350-3360.

Eells, J.T; Wong-Riley, M.T.T.; VerHoeve, J.; Henry, M.; Buchman, E.V.; Kane, M.P.; Goulds, L.J.; Das, R.; Jett, M.; Hodgson, B.D.; Margolis, D. & Whelan, H.T. (2004). Mitochondrial signal transduction in accelerated wound and retinal healing by near-infrared light therapy. *Mitochondrion*, Vol. 4, No. 5-6, 559–567.

Erfurth, S.C. & Peticolas, W.L. (1975). Melting and premelting phenomenon in DNA by laser Raman scattering. *Biopolymers*, Vol. 14, No. 2, 247-264.

Fabian, H. & Mäntele, W. (2002). Infrared Spectroscopy of Proteins, in: *Handbook of Vibrational Spectroscopy*, Chalmers, J.M. & Griffiths, P.R. (Eds.), Vol. 5, 3399-3425, John Wiley & Sons, ISBN 978-0471988472, Chichester.

Falk, M.; Hartman, K. & Lord K. (1963). Hydration of Deoxyribonucleic Acid. II. An Infrared Study. *J. Am. Chem. Soc.*, Vol. 85, No. 4, 387–391.

Fu, F.-N.; DeOliveira, D.B.; Trumble, W.R.; Sarkar, H.K. & Singh, B.R. (1994). Secondary structure estimation of proteins using the amide III region of Fourier Transform

Infrared Spectroscopy: Application to analyze calcium-binding-induced structural changes in calsequestrin. *Appl. Spectrosc.*, Vol. 48, No. 11, 1432-1441.

Fuchs, R.K.; Allen, M.R.; Ruppel, M.E.; Diab, T. ; Phipps, R.J; Miller, L.M. & Burr, D.B. (2008). In situ examination of the time-course for secondary mineralization of Haversian bone using synchrotron Fourier transform infrared microspectroscopy. *Matrix Biol.*, Vol. 27, No. 1, 34-41.

Gąsior-Głogowska, M.; Komorowska, M.; Hanuza, J.; Mączka, M.; Będziński, R.; Kobielarz, M. (2010). Structural alteration of collagen fibers – spectroscopic and mechanic studies. *Acta Bioeng. Biomech.* In preparation.

Gelamo, E.L.; Itri, R.; Alonso, A.; da Silva, J.V. & Tabak, M. (2004). Small-angle X-ray scattering and electron paramagnetic resonance study of the interaction of bovine serum albumin with ionic surfactants. *J. Coll. Interface Sci.*, Vol. 277, No. 2, 471-482.

Gelamo, E.L.; Silva, C.H.T.P.; Imasoto, H. & Tabak, M. (2002). Interaction of bovine (BSA) and human (HSA) serum albumins with ionic surfactants: spectroscopy and modelling. *Biochim. Biophys. Acta*, Vol. 1594, No. 1, 84-99.

Gonzalez, R., Zeng, Y., Ivanov, V. & Zocchi, G. (2009). Bubbles in DNA melting. *J. Phys.: Condens. Matter*, Vol. 21, No. 3, 034102 (9pp).

Goormaghtigh, E.; Cabiaux, V. & Ruysschaert, J.-M. (1990). Secondary structure and dosage of soluble and membrane proteins by attenuated total reflection Fourier-transform infrared spectroscopy on hydrated films. *Eur. J. Biochem.*, Vol. 193, No. 2, 409-420.

Grdadolnik, J. & Maréchal, Y. (2001a). Bovine serum albumin observed by infrared spectrometry. I. Methodology, structural investigation, and water uptake. *Biopolymers (Biospectroscopy)*, Vol. 62, No. 1, 40-53.

Grdadolnik, J. & Maréchal, Y. (2001b). Bovine serum albumin observed by infrared spectrometry. II. Hydration mechanisms and interaction configurations of embedded H(2)O molecules. *Biopolymers (Biospectroscopy)*, Vol. 62, No. 1, 54-67.

Griebe, M.; Daffertshofer, M.; Stroick, M., Syren M., Ahmad-Nejad P., Neumaier M., Backhaus J., Hennerici M.G. & Fatar, M. (2007). Infrared spectroscopy: A new diagnostic tool in Alzheimer disease. *Neurosci. Lett.*, Vol. 420, No. 1, 29-33.

Hackl, E.V.; Kornilova, S.V. & Blagoi, Y.P. (2005). DNA structural transitions induced by divalent metal ions in aqueous solutions. *Int. J. Biol. Macromol.*, Vol. 35, No. 3-4, 175-191.

Hanuza J.; Mączka M.; Gąsior-Głogowska M.; Komorowska M.; Będziński R.; Szotek S.; Maksymowicz K. & Hermanowicz K. (2009). FT-Raman spectroscopic study of thoracic aortic wall subjected to uniaxial stress. *J. Raman Spectrosc., Vol.* 40. In Press.

Harrick, N.J. (1979). *Internal Reflection Spectroscopy*, Vol. 30, Harrick Scientific Corp., ISBN 0933946139, Ossining, New York.

Harris, P.I. & Chapman, D. (1992). Does Fourier-transform infrared spectroscopy provide useful information on protein structures? *Trends Biochem. Sci.*, Vol. 17, No. 9, 328-333.

Heise, H.M.; Küpper, L. & Butvina, L.N. (2002). Bio-analytical applications of mid-infrared spectroscopy using silver halide fiber-optic probes. *Spectrochim. Acta B*, Vol. 57, No. 10, 1649–1663.

Heise, H.M.; Marbach, R.; Janatsch, G. & Kruse-Jarres, J.D. (1989). Multivariate determination of glucose in whole blood by attenuated total reflection infrared spectroscopy. *Anal. Chem.*, Vol. 61, No. 18, 2009-2015.

Ishida, K.P. & Griffiths, P.R. (1993). Comparison of the Amide I/II intensity ratio of solution and solid-state proteins sampled by Transmission, Attenuated Total Reflectance, and Diffuse Reflectance Spectrometry. *Appl. Spectrosc*, Vol. 47, No. 5, 584-589.

Jackson, M. & Mantsch, H.H. (1995). The use and misuse of FTIR spectroscopy in the determination of protein structure. *Crit. Rev. Biochem. Mol. Biol.*, Vol. 30, No. 2, 95-120.

Jackson, M.; Harris, P.I. & Chapman, D. (1989). Fourier transform infrared spectroscopic studies of lipids, polypeptides and proteins. *J. Mol. Struct.*, Vol. 214, 329-355.

Jeyachandran, Y.L.; Mielczarski, E.; Rai, B. & Mielczarski, J.A. (2009). Quantitative and qualitative evaluation of adsorption/desorption of bovine serum albumin on hydrophilic and hydrophobic surfaces. *Langmuir*, Vol. 25, No. 19, 11614-11620.

Jung, Y.M., Czarnik-Matusewicz, B. & Ozaki, Y. (2000). Two-Dimensional Infrared, Two-Dimensional Raman, and Two-Dimensional Infrared and Raman Heterospectral Correlation Studies of Secondary Structure of β-Lactoglobulin in Buffer Solutions. *J. Phys. Chem. B*, Vol. 104, No. 32, 7812–7817.

Keller, P.B. & Hartman, K.A. (1986). Structural forms, stabilities and transitions in double-helical poly(dG-dC) as a function of hydration and NaCl content. An infrared spectroscopic study. *Nucleic Acids Res.*, Vol. 14, No. 20, 8167-8182.

Koening J.L. (2001). *Infrared and Raman Spectroscopy of Polymers.* Rapra Review Reports, Vol. 12, No. 2, Report 134, 2001, iSmithers Rapra Publishing, ISBN 978-1-85957-284-9.

Komorowska, M.; Cuissot, A.; Czarnołęski, A. & Białas, W. (2002a). Erythrocyte response to near-infrared radiation. *J. Photochem. Photobiol., B: Biology*, Vol. 68, No. 2-3, 93-100.

Komorowska, M. & Czyżewska, H. (1997). The effect of Near Infrared radiation on erythrocyte membranes; ESR study. *Nukleonika*, Vol. 42, No. 2, 379-386.

Komorowska, M.; Gałwa, M.; Herter, B. & Wesłowska, U. (2002b). Hydration effects under near-infrared radiation. *Colloids Surf., B.,* Vol. 26, No. 3, 223-233.

Langlais, M.; Tajmir-Riahi, H.A. & Savoie, R. (1990). Raman spectroscopic study of the effects of Ca2+, Mg2+, Zn2+, and Cd2+ ions on calf thymus DNA: binding sites and conformational changes. *Biopolymers*, Vol. 30, No. 7-8, 743-752.

Lee, S.; Debenedetti, P.; Errington, J.; Pethica, B. & Moore, D. (2004). A Calorimetric and Spectroscopic Study of DNA at Low Hydration. *J. Phys. Chem. B*, Vol. 108, No. 9, 3098–3106.

Li, Q.-B.; Sun, X.-J.; Xu, Y.Z.;Yang, L.-M.; Zhang, Y.-F.; Weng, S.-F.; Shi, J.-S. & Wu, J.-G. (2005). Diagnosis of gastric inflammation and malignancy in edoscopic biopsies based on Fourier Transform Infrared Spectroscopy. *Clin. Chem.*, Vol. 51, No. 2, 346-350.

Licoccia, S.; Trombetta, M; Capitani, D.; Proietti, N.; Romagnoli, P. & Di Vona, M.L. (2005). ATR-FTIR and NMR spectroscopic studies on the structure of polymeric gel electrolytes for biomedical applications. *Polymer*, Vol. 46, No. 13, 4670-4675.

Ly, E. Piot, O.; Wolthuis, R.; Durlach, A.; Bernard, P. & Manfait, M. (2008). Combination of FTIR spectral imaging and chemometrics for tumour detection from paraffin-embedded biopsies. *Analyst,* Vol. 133, No. 2, 197–205.

Maréchal, Y. (2004). Observing the water molecule in macromolecules using infrared spectrometry: structure of the hydrogen bond network and hydration mechanism. *J. Mol. Struct.*, Vol. 700, No. 1-3, 217-223.

Maréchal, Y. (2003). Observing the water molecule in macromolecules and aqueous media using infrared spectrometry. *J. Mol. Struct.*, Vol. 648, No. 1-2, 27-47.

Martin, J.C.; Wartell, R.M. & O'Shea, D.C. (1978). Conformational features of distamycin-DNA and netropsin-DNA complexes by Raman spectroscopy. *Proc. Natl. Acad. Sci. USA*, Vol. 75, No. 11, 5483-5487.

Martin, J.C. & Wartell, R.M. (1982). Changes in raman vibrational bands of calf thymus DNA during the B-to-A transition. *Biopolymers*, Vol. 21, No. 3, 499-512.

Matsui, H.; Toyota, N.; Nagatori, M.; Sakamoto, H. & Mizoguchi, K. (2009). Infrared spectroscopic studies on incorporating the effect of metallic ions into a M-DNA double helix. *Phys. Rev. B.*, Vol. 79, 235201-1-235201-8.

Max, J.-J.; Trudel, M. & Chapados, C. (1998). Infrared titration of aqueous glycine. *Appl. Spectrosc.*, Vol. 52, No. 2, 226-233.

McAuley, W.J.; Mader, K.T.; Tetteh, J; Lane, M.E. & Hadgraft, J. (2009). Simultaneous monitoring of drug and solvent diffusion across a model membrane using ATR-FTIR spectroscopy. *Europ. J. Pharmac. Sci.*, Vol. 38, No. 4, 378-383.

Medien, H.A.A. (1998). Spectrophotometric method for determination and kinetics of amino acids through their reaction with syringaldehyde. Spectrochimica Acta A, Vol. 54, No. 2, 359-365.

Meier, R.J. (2005). Vibrational spectroscopy: a 'vanishing' discipline? *Chem. Soc. Rev.*, Vol. 34, 743–752.

Murawska, A.; Cieślik-Boczula, K. & Czarnik-Matusewicz, B. (2010). Interactions in two-component liposomes studied by 2D correlation spectroscopy. *J. Mol. Struct.,* Vol. 974, No. 1-3, 183–191.

Murayama, K.; Wu, Y.; Czarnik-Matusewicz, B. & Ozaki, Y. (2001). Two-Dimensional/Attenuated Total Reflection Infrared Correlation Spectroscopy Studies on Secondary Structural Changes in Human Serum Albumin in Aqueous Solutions: pH-Dependent Structural Changes in the Secondary Structures and in the Hydrogen Bondings of Side Chains. *J. Phys. Chem. B*, Vol. 105, No. 20, 4763-4769.

Noda, I. & Ozaki, Y. (2004). *Two-dimensional Correlation Spectroscopy – Applications in Vibrational and Optical Spectroscopy,* Wiley, ISBN 0-471-62391-1, Chichester.

Noda, I. (2010). Two-dimensional correlation spectroscopy — Biannual survey 2007–2009. *J Mol. Struct.*, Vol. 974, No. 1-3, 3-24.

O'Connor, T.; Mansy, S.; Bina, M.; McMillin, D. R.; Bruck, M.A. & Tobias, R.S. (1982). The pH-dependent structure of calf thymus DNA studied by Raman spectroscopy. *Biophys. Chem.*, Vol. 15, No. 1, 53-64.

Olsztynska-Janus, S.; Szymborska, K.; Komorowska, M. & Lipinski, J. (2009). Conformational changes of L-phenylalanine – Near infrared-induced mechanism of dimerization: B3LYP studies. *J. Mol. Struct. (THEOCHEM)*, Vol. 911, No. 1-3, 1-7.

Olsztynska-Janus, S.; Szymborska, K.; Komorowska, M. & Lipinski, J. (2008), Usefulness of spectroscopy for biomedical engineering. *Acta Bioeng. Biomech.*, Vol. 10, No. 3, 45-49.

Olsztynska, S.; Dupuy, N.; Vrielynck, L. & Komorowska, M. (2006a). Water evaporation analysis of L-phenylalanine from initial aqueous solutions to powder state by vibrational spectroscopy. *Appl. Spectrosc.*, Vol. 60, No. 9, 1040-1053.

Olsztynska, S.; Komorowska, M. & Dupuy, N. (2006b). Influence of Near-Infrared Radiation on the pK_a values of L-phenylalanine. *Appl. Spectrosc.*, Vol. 60, No. 6, 1040-1053.

Olsztynska, S.; Domagalska B.W. & Komorowska, M. (2003). Aggregation of L-phenylalanine amino acid, [in:] *Surfactants and dispersed systems in theory and practice*, Wilk, K.A. (ed.), Oficyna Wydawnicza Politechniki Wrocławskiej, Wrocław, ISBN 83-7085-701-9, 405-409.

Olsztynska, S.; Komorowska, M.; Dupuy, N. & Vrielynck, L. (2001). Vibrational spectroscopic study of L-phenylalanine: Effect of pH. *Appl. Spectrosc.,* Vol. 55, No. 7, 901-907.

Owen, C.A.; Notingher, I.; Hill R.; Stevens, M. & Hench, L.L. (2006). Progress in Raman spectroscopy in the fields of tissue engineering, diagnostics and toxicological testing. *J. Mater. Sci.: Mater. Med.,* Vol. 17, 1019–1023.

Parker, F.S. (1971). Application of infrared spectroscopy in biochemistry, biology and medicine, Plenum Press, ISBN 978-0306305023, New York.

Parker, F.S., (1983). Nucleic Acids and Related Compounds, In: *Applications of Infrared, Raman, and Resonance Raman Spectroscopy in Biochemistry,* 349-398, Plenum Press, ISBN 0-306-41206-3, New York.

Penteado, S.G.; Meneses, C.S; de Oliveira Lobo, A.; Martin, A.A. & da Silva Martinho, H. (2006). Diagnosis of rotator cuff lesions by FT-Raman spectroscopy: a biochemical study. *Presented on SPEC 2006 Shedding Light on Disease: Optical Diagnosis for the New Millenium*, 4th International Conference, 20-24th May, 2006, Heidelberg, Germany

Petrich, W. (2001). Mid-Infrared and Raman Spectroscopy for Medical Diagnostics. *Appl. Spectrosc. Rev*., Vol. 36, No. 2&3, 181-237.

Pevsner, A. & Diem, M. (2001). Infrared spectroscopic studies of major cellular components. Part I: The effect of hydration on the spectra of proteins. *Appl. Spectrosc.,* Vol. 55, No. 6, 788-793.

Pevsner, A. & Diem, M. (2003). IR spectroscopic studies of major cellular components. III. Hydration of protein, nucleic acid, and phospholipid films. *Biopolymers,* Vol. 72, No. 4, 282-289.

Pilet, J. & Brahms, J. (1973). Investigation of DNA structural changes by infrared spectroscopy. *Biopolymers*, Vol. 12, No. 2, 387-403.

Pohle, W. & Fritzsche, H. (1980). A new conformation-specific infrared band of A-DNA in films. *Nucleic Acids Res.*, Vol. 8, No. 11, 2527–2535.

Posten, W.; Wronde, D.A.; Dover, J.S.; Arndt, K.A.; Silapunt, S. & Alam, M. (2005). Low-level laser therapy for wound healing: mechanism and efficacy. *Dermatol. Surg.*, Vol. 31, No. 3, 334-340.

Prescott, B.; Steinmetz, W. & Thomas Jr, G.J. (1984). Characterization of DNA structures by laser Raman spectroscopy. *Biopolymers*, Vol. 23, No. 2, 235-256.

Prestrelski S.J.; Byler, D.M. & Thompson, M.P. (1991). Effect of metal ion binding on the secondary structure of bovine α-lactalbumin as examined by infrared spectroscopy. *Biochemistry*, Vol. 30, No. 36, 8797-8804.

Pysz, M.A.; Gambhir, S.S. & Willmann, J.K. (2010). Molecular imaging: current status and emerging strategies. *Clin. Radiol.*, Vol. 65, No. 7, 500-516.

Qing, H; He Yanlin, H.; Fenlin, S. & Zuyi, T. (1996), Effect of pH and metal ions on the conformation of bovine serum albumin in aqueous solution. An attenuated total reflection (ATR) FTIR spectroscopic study. *Spectrochim. Acta A*, Volume 52, No. 13, 1795-1800.

Rauch, C.; Pichler, A.; Trieb, M.; Wellenzohn, B.; Liedl, R.K. & Mayer, E. (2005). Z-DNA's Conformer Substates Revealed by FT-IR Difference Spectroscopy of Nonoriented Left-Handed Double Helical Poly(dG-dC). *J. Biomol. Struct. Dyn.*, Vol. 22, No. 5, 595-614.

Shanmugam, G. & Polavarapu, P.L. (2006). Structures of intact glycoproteins from vibrational circular dichroism. *Proteins*, Vol. 63, No. 4, 768-776.

Sieroń, A.; Cieślar, G, & Adamek, M. (1994). *Magnetotherapy and lasertherapy*, Polish ed., Silesian Academy of Medicine, ISBN 8390110776, Katowice.

Silver, F.H.; Freeman, J.W. & Seehra, G.P. (2003). Collagen self-assembly and the development of tendon mechanical properties. *J. Biomech., Vol.* 36, No. 10, 1529-1553.

Sirichaisit, J.; Young, R.J. & Vollrath, F. (2000). Molecular deformation in spider dragline silk subjected to stress. *Polymer*, Vol. 41, No. 3, 1223-1227.

Smith, B. M.; Oswald, L. & Franzen, S. (2002). Single-Pass Attenuated Total Reflection Fourier Transform Infrared Spectroscopy for the Prediction of Protein Secondary Structure. *Anal. Chem.*, Vol. 74, No. 14, 3386-3391.

Sun, X.-J.; Su, Y.-L.; Soloway, R.D.; Zhang, L.; Wang, J.-S.; Ren, Y.; Yang L.-M.; Zheng, A.-G.; Zhang, Y.-F; Xu, Y.-Z.; Weng, S.-F.; Shi, J.-S.; Xu, D.-F. & Wu, J.-G. (2003). Rapid, intraoperative detection of malignancy using attenuated total reflectance (ATR) and mobile Fourier transform infrared (FT-IR) spectroscopy. *Gastroenterology*, Vol. 124 (Suppl.), No. 4, Suppl.1, A420-A421.

Sun, C.; Yang, J.; Wu, X.; Huang, X.; Wang F. & Liu, S. (2005). Unfolding and refolding of bovine serum albumin induced by cetylpyridinium bromide. *Biophys. J.*, Vol. 88, No. 5, 3518-3524.

Synytsya, A.; Alexa, P.; de Boer, J.; Loewe, M.; Moosburger, M.; Wurkner, M. & Volka, K. (2007). Raman spectroscopic study of calf thymus DNA: an effect of proton- and γ-irradiation. *J. Raman Spectr.*, Vol. 38, No. 14, 1406-1415

Szwed, J.; Cieślik-Boczula, K.; Czarnik-Matusewicz, B.; Jaszczyszyn, A., Gąsiorowski, K.; Świątek, P. & Malinka, W. (2010). Moving-window 2D correlation spectroscopy in

studies of fluphenazine–DPPC dehydrated film as a function of temperature. *J. Mol. Struct*., Vol. 974, No. 1-3, 192–202.

Szyc, Ł.; Pilorz, S. & Czarnik-Matusewicz, B. (2008). FTIR-ATR investigations of an alpha-helix to beta-sheet conformational transition in poly(L-lysine). *J. Mol. Liq.,* Vol. 141, No. 3, 155-159.

Szymborska-Małek, K.; Czarnik-Matusewicz, B. & Komorowska M. (2009a). Two-dimensional correlation analysis in studies of influence of NIR radiation on thin film of DNA measured by FTIR-ATR spectroscopy. *Book of Abstracts of The Fifth International Symposium on Two-Dimensional Correlation Spectroscopy*, pp. 54, Wroclaw, August 2009, Poland; and article in preparation.

Szymborska-Małek, K.; Czarnik-Matusewicz, B. & Komorowska M. (2009b). Study of influence of NIR radiation on herring sperm DNA by ATR-FTIR, UV spectroscopies and DSC. *Book of Abstracts of XIII European Conference on the Spectroscopy of Biological Molecules*, pp. 53, Palermo, August 2009, Italy; and article in preparation.

Taboury, J. A.; Liquier, J. & Taillandier, E. (1985). Characterization of DNA structures by infrared spectroscopy: double helical forms of poly(dG–dC) • poly(dG–dC), poly(dD8G–dC) • poly(dD8G–dC), and poly(dG–dm5C) • poly(dG–dm5C). *Can. J. Chem*., Vol. 63, No. 7, 1904–1909.

Taillandier, E.; Liquier, J. & Ghomi, M. (1989). Conformational transitions of nucleic acids studied by IR and Raman spectroscopies. *J. Mol. Struct.*, Vol. 214, 185-211.

Taillandier, E. & Liquier, J. (1992). Infrared spectroscopy of DNA. *Methods Enzymol.*, Vol. 211, 307-335.

Tajmir-Riahi, H. A.; Ahmad, R.; Naoui, M. & Diamantoglou S. (1995). The effect of HCl on the solution structure of calf thymus DNA: a comparative study of DNA denaturation by proton and metal cations using Fourier transform IR difference spectroscopy. *Biopolymers*, Vol. 35, No. 5, 493-501.

Tao, N.; Lindsay, S. & Rupprecht, A. (1989). Structure of DNA hydration shells studied by Raman spectroscopy. *Biopolymers*, Vol. 28, No. 5, 1019-1030.

Van de Weert, M.; Harris, P.I.; Hennink, W.E. & Crommelin, D.J.A. (2001). Fourier Transform Infrared Spectrometric Analysis of Protein Conformation: Effect of Sampling Method and Stress Factors. *Anal. Biochem.*, Vol. 297, No. 2, 160-169.

Wang Y.-N.; Galiotis C. & Bader D.L. (2000). Determination of molecular changes in soft tissues under strain using laser Raman microscopy. *J. Biomech.*, Vol. 33, No. 4, 483-486.

Wang, S.-L.; Wei, Y.-S. & Lin, S.-Y. (2003). Subtractive similarity method used to study the infrared spectra of proteins in aqueous solution. *Vib. Spectrosc.*, Vol. 31, No. 2, 313-319.

Wartewig, S. & Neubert, R.H. (2005). Pharmaceutical applications of Mid-IR and Raman spectroscopy. *Adv. Drug Deliv. Rev.*, Vol. 57, No. 8, 1144-1170.

Winchester M.W., Winchester L.W., Chou N.Y. (2008). Application of Raman Scattering to the Measurement of Ligament Tension. *Conference Proceedings: Engineering in Medicine and Biology Society*, pp.3434–3437, 30th Annual International Conference of the IEEE, 14th October, 2008, Vancouver.

Wolpert, M. & Hellwig, P. (2006). Infrared spectra and molar absorption coefficients of the 20 alpha amino acids in aqueous solutions in the spectral range from 1800 to 500 cm^{-1}. *Spectrochim. Acta A*, Vol. 64, No. 4, 987-1001.

Wood, B.R.; Tait B. & Mcnaughton, D. (2000). Fourier Transform Infrared Spectroscopy as a Method for Monitoring the Molecular Dynamics of Lymphocyte Activation. *Appl. Spectrosc.*, Vol. 54, No. 3, 353-359.

Wu, Y.; Murayama, K.; Czarnik-Matusewicz, B. & Ozaki, Y. (2002). Two-Dimensional Attenuated Total Reflection/Infrared Correlation Spectroscopy Studies on Concentration and Heat-Induced Structural Changes of Human Serum Albumin in Aqueous Solutions. *Appl. Spectrosc.*, Vol. 56, No. 9, 1186-1193.

Wu, Y.; Czarnik-Matusewicz, B.; Murayama, K. & Ozaki, Y. (2000). Two-Dimensional Near-Infrared Spectroscopy Study of Human Serum Albumin in Aqueous Solutions: Using Overtones and Combination Modes to Monitor Temperature-Dependent Changes in the Secondary Structure. *J. Phys. Chem. B*, Vol. 104, No. 24, 5840-5847.

Zhang, J. & Yan, Y.-B. (2005). Probing conformational changes of proteins by quantitative second derivative infrared spectroscopy. *Anal. Biochem.*, Vol. 340, No. 1, 89-98.

Biomedical Engineering, Trends, Research and Technologies

Edited by Dr. Sylwia Olsztynska

ISBN 978-953-307-514-3
Hard cover, 644 pages
Publisher InTech
Published online 08, January, 2011
Published in print edition January, 2011

This book is addressed to scientists and professionals working in the wide area of biomedical engineering, from biochemistry and pharmacy to medicine and clinical engineering. The panorama of problems presented in this volume may be of special interest for young scientists, looking for innovative technologies and new trends in biomedical engineering.

How to reference

In order to correctly reference this scholarly work, feel free to copy and paste the following:

Sylwia Olsztyńska-Janus, Marlena Gąsior-Głogowska, Katarzyna Szymborska-Małek, Bogusława Czarnik-Matusewicz and Małgorzata Komorowska (2011). Specific Applications of Vibrational Spectroscopy in Biomedical Engineering, Biomedical Engineering, Trends, Research and Technologies, Dr. Sylwia Olsztynska (Ed.), ISBN: 978-953-307-514-3, InTech, Available from: http://www.intechopen.com/books/biomedical-engineering-trends-research-and-technologies/specific-applications-of-vibrational-spectroscopy-in-biomedical-engineering

INTECH
open science | open minds

InTech Europe
University Campus STeP Ri
Slavka Krautzeka 83/A
51000 Rijeka, Croatia
Phone: +385 (51) 770 447
Fax: +385 (51) 686 166
www.intechopen.com

InTech China
Unit 405, Office Block, Hotel Equatorial Shanghai
No.65, Yan An Road (West), Shanghai, 200040, China
中国上海市延安西路65号上海国际贵都大饭店办公楼405单元
Phone: +86-21-62489820
Fax: +86-21-62489821